Ultra-High-Q Racetrack Resonators on Thick SOI Platform Through Hydrogen Annealing Smoothing

Yisbel E. Marin, Arijit Bera, Matteo Cherchi, and Timo Aalto

***Abstract*—We implemented a hydrogen annealing based post-processing technique as a tool to improve the sidewall roughness of 3 μm thick silicon-on-insulator (SOI) waveguides and demonstrated ultra-high-*Q* factors on racetrack resonators leveraging on the propagation loss reduction achieved through the smoothing process. The designed racetracks are based on a combination of rib waveguides and strip-waveguide-based Euler bends. We measured intrinsic quality factors of 14 $\times$ 10^6 for a racetrack with a footprint of $\sim$5.5 mm^2 and 10.7 $\times$ 10^6 for a smaller racetrack with footprint of $\sim$1.48 mm^2. The estimated propagation loss for the rib waveguides was $\sim$2.7 dB/m, representing a $\times$3 reduction respect to the previously measured losses of 3 μm thick SOI rib waveguides treated with thermal oxidation smoothing. Overall, the post-processing technique allowed to significantly reduce the sidewall roughness without altering the geometry of the waveguides, unlike in sub-micron scale SOI platforms, making it an attractive solution for applications demanding ultra-low losses.**

***Index Terms*—Hydrogen annealing, low-loss waveguides, microresonators, optical losses, photonic integrated circuits, resonators, sidewall roughness, silicon photonics.**

I. Introduction

SILICON-ON-INSULATOR (SOI) technology has enabled a myriad of photonics applications leveraging on its CMOS compatibility and high integration density capability thanks to the high index contrast of its waveguides. This very characteristic plays an important role in the relatively high propagation losses of SOI waveguides, since it enhances the interaction of the optical field with the sidewall roughness introduced during fabrication processes such as lithography and etching [1]. This interaction is particularly strong in sub-micron scale waveguides see Fig. 1(a), producing losses of a few dB/cm [2], whereas for thicker Si layers, such as in the 3 μm thick SOI platform, the field has a higher confinement factor due to its larger core size (see Fig. 1), resulting in very low propagation losses [3].

Many emerging applications rely on the filtering and energy storing and enhancing properties of integrated resonators. They are used in lasers for linewidth suppression [4], in nonlinear photonics for enhancement of nonlinear interaction in frequency comb generation [5] and Brillouin lasers [6], in microwave photonics for signal processing [7], and, more recently, in quantum photonics, for communications [8] and metrology [9], among others. All of these applications require very narrow linewidths and low propagation losses, therefore a high quality (*Q*-) factor. The relation between the cavity losses, including waveguide propagation losses, and the intrinsic *Q*-factor of a resonator is inverse [10]. Efforts towards demonstrating high *Q*-factors on SOI technology have mainly revolved around reducing the field interaction with the sidewall roughness to in turn reduce the

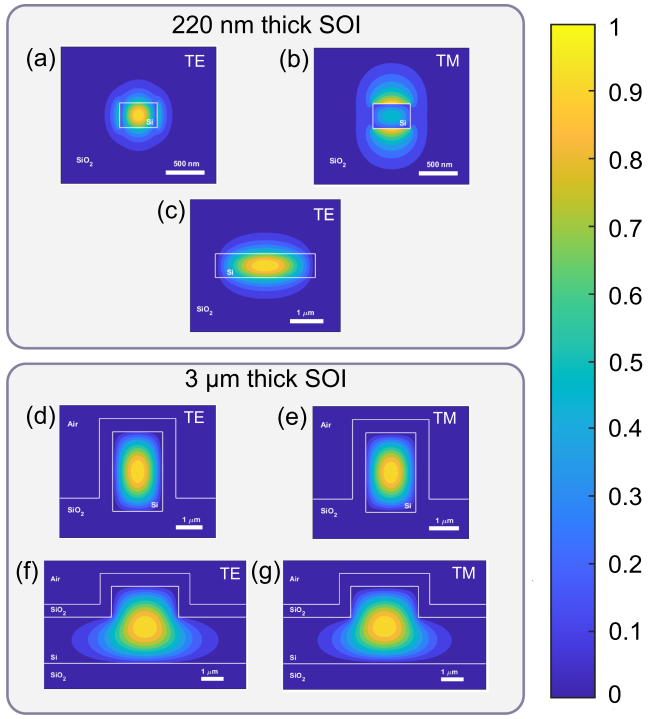

Fig. 1. Mode comparison for SOI platforms with different Si thicknesses. In 220 nm thick SOI SM waveguides (width = 450 nm) the (a) TE mode (n_{eff} = 2.3541) has a confinement factor (CF) of 0.7373 and (b) TM (n_{eff} = 1.7238) a CF = 0.4108. (c) For MM waveguides of the same thickness and width = 3 μm the fundamental TE mode (n_{eff} = 2.8368) has a higher CF = 0.8110. For a 3 μm thick SOI strip MM waveguide (width = 1.875 μm) the field is very confined for both (d) fundamental TE (n_{eff} = 3.4439) with CF = 0.9995 and (e) fundamental TM (n_{eff} = 3.4461) CF = 0.9988. For 3 μm wide SM rib waveguides of the same thickness the field is also well confined for (f) TE (n_{eff} = 3.4619) with CF = 0.9995 and (g) TM (n_{eff} = 3.4612) CF = 0.9997. All the modes were calculated at a wavelength of 1.55 μm. CF: ratio of the field within the core region to the field within the whole waveguide structure.

Manuscript received 15 December 2022; revised 28 February 2023 and 21 March 2023; accepted 23 March 2023. Date of publication 27 March 2023; date of current version 9 June 2023. This work was supported in part by PICAP Project through Business Finland under Grant 44065/31/2020 and in part by the Academy of Finland Flagship Programme, Photonics Research and Innovation (PREIN) under Grant 320168. *(Corresponding author: Yisbel E. Marin).*

The authors are with the VTT Technical Research Centre of Finland, 02044 Espoo, Finland (e-mail: yisbel.marin@vtt.fi; arijit.bera@vtt.fi; matteo.cherchi@vtt.fi; timo.aalto@vtt.fi).

Color versions of one or more figures in this article are available at https://doi.org/10.1109/JLT.2023.3262413.

Digital Object Identifier 10.1109/JLT.2023.3262413

scattering losses. By increasing the width in sub-micron SOI waveguides, it is possible to reduce the scattering losses, however, by doing so, the waveguides become multimodal, so care must be taken to avoid higher order mode (HOM) excitation. One approach to avoid HOM excitation is to restrict the use of multimode (MM) waveguides to the straight sections of the racetrack and use single-mode (SM) waveguides for the bend sections, which also allows to achieve tight bending radii. Following this configuration, a compact racetrack used a combination of 2 μm wide MM and 500 nm SM ridge waveguides on 220 nm thick SOI to demonstrate a Q-factor of 1.1×10^6 and propagation loss down to 0.21 dB/cm [11]. Similarly, a Q-factor of 1.6×10^6 was measured for a large-area racetrack on 220 nm thick SOI using 3 μm wide MM rib waveguides and 500 nm wide SM strip waveguides in the coupling and bend sections. The propagation losses of the MM waveguides were as low as 8.5 dB/m, however the Q-factor was reduced by loss contributions from the adiabatic directional coupler, adiabatic bends and strip-to-rib conversion tapers [12], therefore avoiding this transition between different waveguide types could improve the performance. In resonators based only on MM waveguides the bends must be designed following a curve that prevents or minimizes HOMs excitation, since the Q-factor can be degraded in parts of the spectrum where the resonances of the fundamental mode and HOMs are close and the intermodal crosstalk is sufficiently high [13]. Racetracks incorporating so-called Euler bends can provide very low intermodal crosstalk. A racetrack based on 1.6 μm wide MM strip waveguides on 220 nm thick SOI achieved a 2.3×10^6 intrinsic Q-factor and estimated waveguide loss of 0.3 dB/cm by implementing Euler bends with an intermodal crosstalk bellow -30 dB between 1500 nm and 1600 nm [14]. A racetrack using a modified version of the Euler bend has also been proposed, showing a Q-factor of 10.2×10^6. The estimated propagation losses for the used 3 μm wide by 220 nm thick strip SOI waveguides was down to 6.5 dB/m. For waveguides this wide, the field interaction with the sidewall roughness is greatly minimized, as it can be seen in Fig. 1(c), however the losses are still limited by the sidewall roughness, which could be improved by optimizing the fabrication methods [15]. A different configuration to avoid HOM excitation used MM concentric racetracks combined with a broadband directional coupler based on a pulley configuration demonstrating a Q-factor of 1.4×10^6 over a wavelength range from 1240 to 1680 nm. The two supermodes of the concentric waveguides had slightly detuned resonance wavelengths, which helps counteract the Q-factor deterioration due to coupling to HOMs at the fundamental mode resonances [16].

Another approach to achieve high Q-factors is to smoothen the sidewall roughness through different processing techniques. A combination of surface smoothing through oxidation and resist reflow to improve the etch mask pattern allowed to demonstrate an internal Q-factor of 22×10^6 using a ring resonator based on shallow-etched rib waveguides. Besides the improvements obtained through processing, the geometry of the waveguides reduces the field interaction with the sidewalls, translating into losses of 2.7 dB/m, however to limit the contribution from bending losses a large radius of 2.45 mm was needed [17]. In 3 μm thick SOI high intrinsic Q-factors have been demonstrated through the combination of large cross-section waveguides and thermal oxidation (TOX) smoothing post-processing [18]. A Q-factor of 8×10^6 was demonstrated for a ring resonator based on SM rib waveguides, with a radius of 2.6 mm (21 mm^2 footprint). A more compact racetrack configuration was achieved by combining the same type of rib waveguides for the straight sections and MM strip waveguides for the bend sections, resulting in an intrinsic Q of 4.3×10^6. In both configurations the Q-factor was limited by the propagation losses of $\sim$0.1 dB/cm. The TOX process has some drawbacks, such as linewidth reduction, introduction of surface stress [19], and rounding at the inner corners of the waveguides, which can be detrimental to the performance of some devices. Additionally, it is desirable to further reduce the scattering losses of silicon waveguides beyond what has already been demonstrated in this platform.

In this work we implement a hydrogen annealing based post-processing technique to smoothen the sidewall roughness of 3 μm thick SOI waveguides and reduce the propagation losses. This process was originally proposed in the MEMS field [20] and it was later used to smoothen sub-micron scale SOI waveguides [21], enabling losses down to 0.1 dB/cm in the C-band [22]. However, for waveguides at this size scale preserving the shape and dimensions can be challenging [19]. We have previously demonstrated propagation losses of $\sim$4 dB/m in strip waveguides on thick SOI through this process [23]. Here we exploit this result to demonstrate ultra-high Q resonators. We designed two racetracks with footprints of $\sim$1.48 mm^2 and $\sim$5.5 mm^2 [24]. The smaller racetrack had an intrinsic Q-factor of 10.7×10^6 and the larger one 14.3×10^6, corresponding to a loss for the rib waveguides of $\sim$2.7 dB/m. These results are an improvement respect to the ones obtained through TOX in [18], while requiring a much smaller footprint. Additionally, the devices were fabricated in a multi-project wafer (MPW) run, meaning that the process is completely compatible with our current open-access fabrication process, hence it can be integrated into the process flow, enabling new applications that could benefit from the demonstrated ultra-low losses.

II. Design

A schematic of the proposed add-drop racetrack configuration is shown in Fig. 2(a). The straight sections consist of rib waveguides with a width of 3 μm and etch depth of 1.2 μm. These dimensions guarantee a single-mode operation [25] over an ultra-broad wavelength range (1.2-4 μm), along with ultra-low propagation loss [3] thanks to the field being so well confined inside the core see Fig. 1(f)–(g). Rib waveguides have high bending losses due to radiative coupling of HOMs into the slab, therefore requiring a large bending radius for the resonator losses to be dominated by the propagation losses [18]. To circumvent this, we used strip waveguides for the bends. The single mode operation of 3 μm thick Si strip waveguides would require sub-micron widths, resulting in a high aspect ratio which makes waveguides prone to cracking due to stress, and also leads to higher propagation losses, due to the field being less confined inside the core. Increasing the width to a micron scale results in multi-mode operation, therefore an arc bend would require

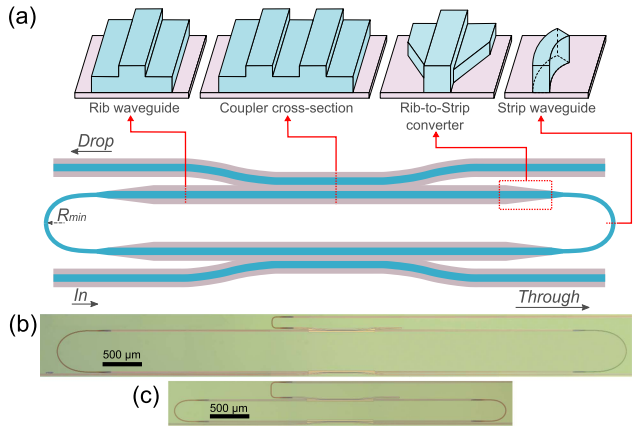

Fig. 2. (a) Schematic of the racetrack configuration. Straight and coupling sections are based on single-mode rib waveguides, whereas the bends are based on multi-mode strip waveguides following an Euler curve. (b) Microscope image of the racetrack with $R_{\min} = 194.87$ μm. (c) Microscope image of the racetrack with $R_{\min} = 97.32$ μm.

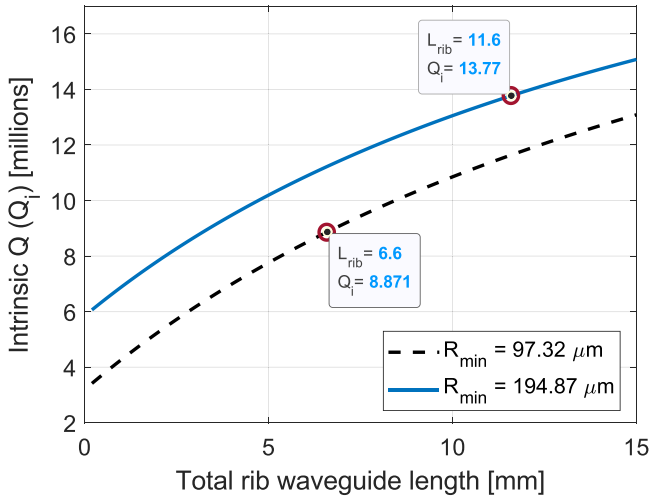

Fig. 3. Estimated intrinsic Q (Q_i) versus the total length of the straight rib waveguide section (L_{rib}) for the racetracks with minimum bend radii of 97.32 μm and 194.87 μm.

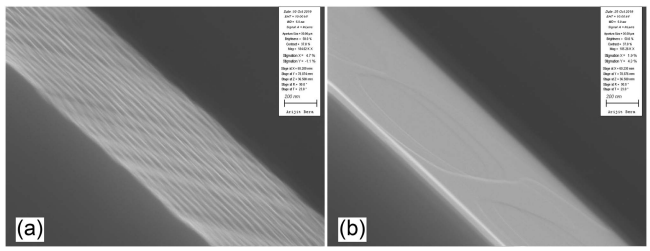

Fig. 4. Scanning electron microscope (SEM) images of waveguide-like test structures processed on 3 μm thick Si monitor wafers (a) before and (b) after H_2 annealing for 15 minutes in an 80 Torr pressure at 900 °C.

a large radius to avoid HOM excitation, unless a configuration such as the so-called "matched bends" is used. However, this approach does not allow to achieve a very small radius and provides a limited wavelength range of operation [26]. To guarantee that the power of the fundamental mode coupled at the input of the bend is in turn coupled to the fundamental mode of the waveguide at its output, while using a tight bending radius, the bends of the proposed racetrack follow a so-called Euler curve. This type of bend has been successfully demonstrated on VTT's thick SOI platform with very low losses in a wide wavelength range and supporting both TE and TM polarizations [27]. For the coupling sections, we used a directional coupler based on rib waveguides (see Fig. 2(a)) since on thick SOI the strong field confinement prevents efficient enough coupling between strip waveguides (see Fig. 1(d)–(e)).

To determine the optimal bend radii for the 180° Euler (U-) bend, we simulated the transmission for different radii following the procedure detailed in [27] using FIMMPROP. We designed a so-called large racetrack (shown in Fig. 2(b)) with a minimum radius $R_{\min} = 194.87$ μm (effective radius $R_{\text{eff}} = 268.9$ μm) for a transmission of 99.98% in the fundamental mode, and a so-called small racetrack (see Fig. 2(c)) with $R_{\min} = 97.3$ μm ($R_{\text{eff}} = 134.3$ μm) for a transmission of 99.91% in the fundamental mode. For the transition between the straight and bend sections we used rib-to-strip converters (see Fig. 2(a)) to couple the fundamental mode of the SM rib waveguide to the fundamental mode of the MM strip waveguide. The converters are characterized by a length of 200 μm and an insertion loss of ~0.014 dB per converter [14]. Fig. 3 shows the estimation of the intrinsic Q versus the total length of straight rib waveguide sections of the racetrack, considering the previously mentioned bend radii and converter length. To estimate the intrinsic or loss Q, we need to know the propagation loss of the rib waveguides after hydrogen annealing smoothing. The losses measured for rib waveguides processed with TOX smoothing are 0.1 dB/cm [3], and we have also demonstrated a ×3 reduction of the propagation loss in strip waveguides through hydrogen annealing [23], therefore we assumed a loss for the ribs of ~0.03 dB/cm. From these estimations, we chose a total rib waveguide length $L_{\text{rib}} = 11.6$ mm for the large racetrack to obtain an estimated 13.77×10^6 intrinsic Q and free spectral range FSR = 5.3 GHz. For the smaller racetrack we chose $L_{\text{rib}} = 6.6$ mm for an intrinsic Q of 8.87×10^6 and FSR = 9.1 GHz.

Regarding the external coupling to the cavities, the target was to design weakly coupled racetracks, so that the Q of the resonator was dominated by the propagation losses of the waveguides. However, since the exact propagation losses of the rib waveguides after the H_2 annealing process were unknown, racetracks with identical cavities but different coupling coefficients (different gap between waveguides in the directional coupler) were cascaded, sharing the same input bus (see diagrams in Figs. 8(a) and 9(a)).

III. Fabrication

The devices were fabricated in an MPW run at VTT. The waveguides were defined on 3 μm thick silicon wafers using stepper lithography (i-line), followed by inductively coupled plasma – reactive ion etching (ICP-RIE) with a Bosch process [28]. This type of etching leads to scallop formation on the sidewall, that adds to the roughness already introduced during lithography (see Fig. 4(a)). Next, the wafer was annealed in

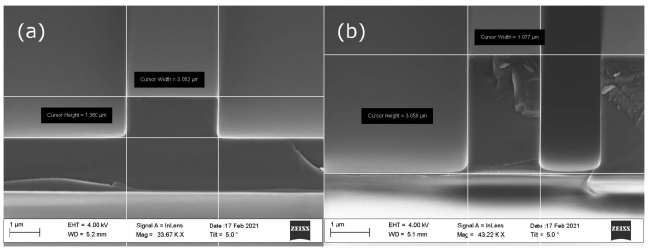

Fig. 5. SEM images after H_2 annealing of a (a) rib waveguide with nominal width of 3 μm, height of 3 μm and etching depth of 1.2 μm, and (b) strip waveguide with nominal width of 1.875 μm and height of 3 μm.

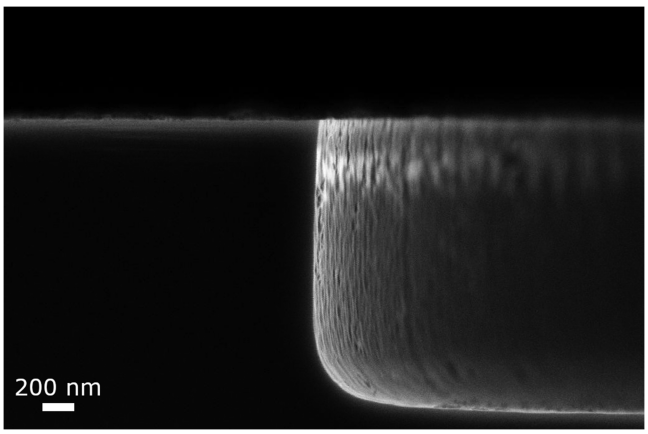

Fig. 6. SEM image of a 3 μm thick Si rib waveguide after thermal oxidation.

an epi-reactor within 100% pure hydrogen atmosphere, with a pressure of 70 Torr at 900 °C for 15 min. These annealing parameters allowed to significantly smoothen the sidewall roughness, as seen in Fig. 4(b) for waveguide-like test structures processed on silicon monitor wafers for optimization of the annealing process. The dimensions and geometry of the waveguides were also preserved, as shown in Fig. 5(a) for rib waveguides (targeted width = 3 μm) and 5.b for strip waveguides (targeted width = 1.875 μm). These results show an improvement over the sidewall smoothing by thermal oxidation, which in contrast affects the linewidth and results in rounding at the inner corners of the rib waveguides, as evidenced in Fig. 6. The final fabrication step was deposition of a 0.5 μm thick TEOS cladding layer on top of the waveguides through LPCVD.

IV. Experimental Results

The measurement setup is shown in Fig. 7. The optical source was the tunable laser TSL-550 by Santec, characterized by a 200 kHz linewidth. For the detection we used a power meter module MPM-211, also by Santec. The Si waveguides support both TE and TM polarizations, therefore careful coupling of the desired single polarization into the chip is required. For this, we used a polarization control stage consisting of a fiber polarization controller, which rotates the polarized light with arbitrary angle at the input into 45 degrees at the output, followed by a switch that routes the input light into one of two outputs. Each of these outputs is connected to a fiber optic polarizing beam splitter,

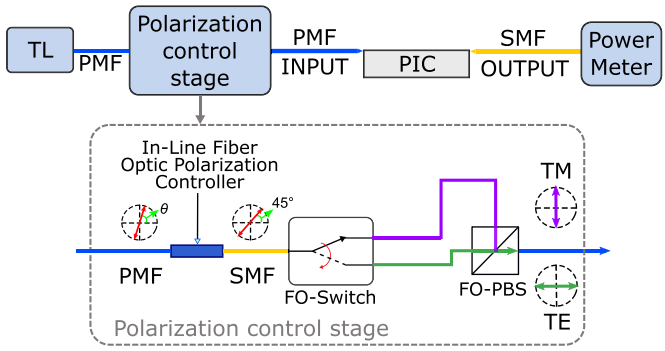

Fig. 7. Experimental setup schematic. TL: tunable laser, SMF: single mode fiber, PMF: polarization maintaining fiber, FO-Switch: fiber optic switch, FO-PBS: fiber optic polarizing beam splitter. θ: arbitrary angle of the polarized light at the input.

so according to the switch state either TE or TM polarization is obtained at the output. The whole stage has a polarization extinction ratio of ~20 dB. To couple the light into the chip through edge coupling we used tapered fibers to approximately match the mode size of the Si rib waveguides at the facets of the chip. A polarization maintaining fiber was used at the input, whereas a standard single-mode fiber was used at the output.

The transmission spectra for TM and TE polarization at the through and drop ports are shown in Fig. 8, for the large racetrack, and Fig. 9, for the small racetrack. The measured FSRs were 5.6 GHz and 9.6 GHz respectively. We can observe the presence of off-resonance notches that are stronger than others in the through spectra of both racetracks (pointed out with an encircled 2 and 2/3 in Figs. 8 and 9 respectively), which are not aligned with the drop port resonance peaks. These actually correspond to the resonance of cascaded resonators that share the same through port as the devices under test as explained in section II. We can also see in Fig. 8(b) the presence of off-resonance peaks for the TE polarization. These likely belong to a HOM since the measured rib waveguides were slightly over-etched to a depth of ~1.4 μm instead of the target depth of 1.2 μm, making the rib waveguide slightly multimodal, capable of supporting a higher order TE mode. However, the extinction ratio between this and the fundamental mode resonances is >20 dB and we did not notice significant induced asymmetry of the fundamental mode resonances. For the large racetracks there were two cascaded racetracks, as shown in Fig. 8(a), whereas for the smaller racetracks there were three of them as shown in Fig. 9(a). Here we show the results for the racetracks with weaker coupling coefficients (larger coupler gap).

The linewidths and Q-factors of the resonance peaks were extracted following temporal coupled-mode theory. According to this, the transmission spectrum of an add-drop resonator is given by the coupled-mode equation solution [29]:

$$\left|\frac{s_{drop}}{s_{in}}\right|^2 = \frac{4\gamma_{ext}^2}{(\omega-\omega_0)^2+\gamma_T^2}, \tag{1}$$

where $|s_{drop}|^2$ is the power at the drop port, $|s_{\mathrm{in}}|^2$ is the power at the input port, γ_{ext} is the external coupling rate, ω_0 is the angular resonance frequency, and γ_{T} is the total linewidth given

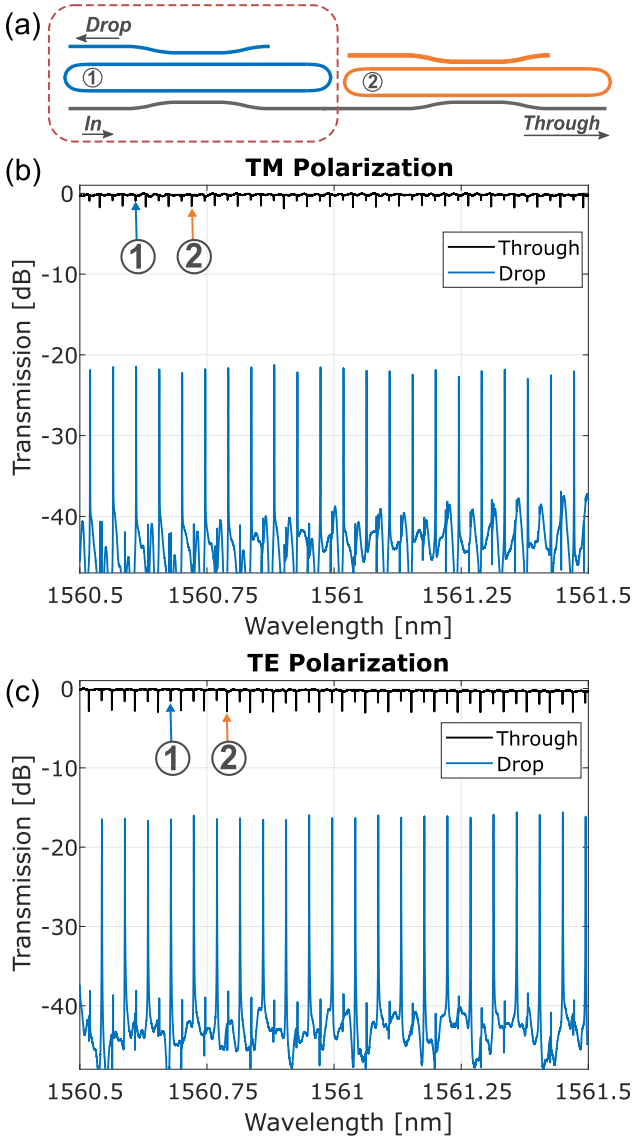

Fig. 8. (a) Cascaded large racetracks with identical cavity dimensions, but different directional coupler gaps. The drop spectra in (b) for TM and (c) for TE polarization correspond to the first racetrack with larger gap, hence lower coupling coefficient (enclosed in red dashed lines in (a)). The pointer one indicates a resonance corresponding to the first racetrack and pointer 2 to the second.

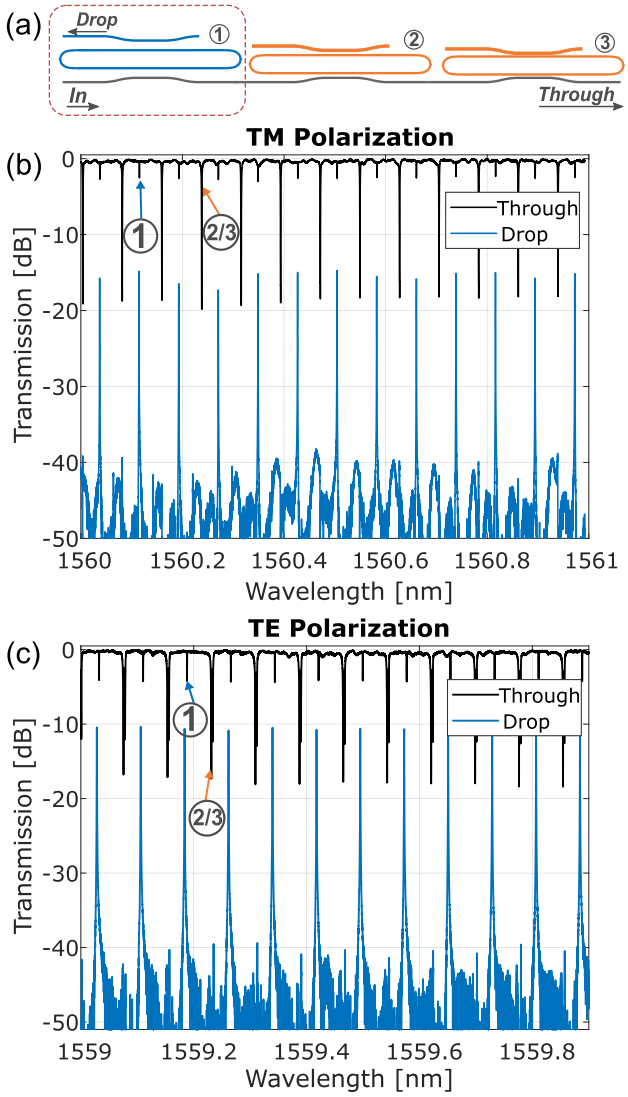

Fig. 9. (a) Cascaded small racetracks with identical cavity parameters, except with different gaps to achieve different coupling coefficients. The drop spectra in (b) for TM and (c) for TE polarization were measured from the first racetrack with larger gap (enclosed in red dashed lines in (a)). The pointer one indicates a resonance of the first racetrack and the pointer 2/3 resonances of the second and third racetrack.

by:

$$\gamma_{\mathrm{T}} = \gamma_{\mathrm{ext}} + \gamma_{\mathrm{i}}, \tag{2}$$

where γ_{i} is the intrinsic linewidth. The loaded Q-factor $Q_{\mathrm{T}} = \omega_0/\gamma_{\mathrm{T}}$ is then estimated by performing Lorentzian fit of the resonance peaks at the drop port based on (1), which also allowed to extract the external Q-factor $Q_{\mathrm{ext}} = \omega_0/\gamma_{\mathrm{ext}}$, and therefore the intrinsic or internal Q-factor $Q_{\mathrm{i}} = \omega_0/\gamma_{\mathrm{i}}$ from (2).

The calculated mean intrinsic Q of the large racetrack between 1560.5 nm and 1561.5 nm for TM was 12.2×10^6, with a maximum value of 14.3×10^6 at 1560.61 nm, corresponding to a linewidth of 0.12 pm (14.84 MHz), as shown in Fig. 10(a), whereas for TE polarization the mean Q_{i} was 9.2×10^6, with a maximum of 12.7×10^6 at 1561.13 nm, corresponding to a linewidth of 0.14 pm (17.77 MHz), as shown in Fig. 10(b). For the small racetrack the mean intrinsic Q between 1560 nm and 1561 nm for TM polarization was 9.2×10^6, with a maximum value of 10.7×10^6 at 1560.58 nm, corresponding to a linewidth of 0.18 pm (21.80 MHz), as shown in Fig. 11(a), and for TE the mean between 1559 nm and 1560 was 7.1×10^6, with a maximum of 8.2×10^6 at 1559.26 nm, as shown in Fig. 11(b). The slightly higher Q for TM compared to TE for both racetracks is likely due to the stronger confinement of the optical field for TM, since this leads to less interaction with the sidewall roughness, and therefore, lower scattering losses. The estimated propagation loss extracted from the measured maximum intrinsic Q was down to ~2.7 dB/m. These results are in good agreement with the estimations from Section II.

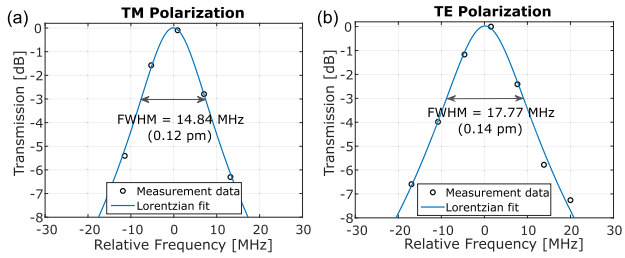

Fig. 10. Resonance peak with highest intrinsic Q (narrower linewidth) for the large racetrack: (a) TM and (b) TE polarization.

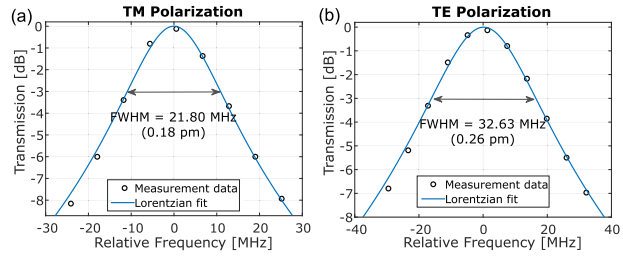

Fig. 11. Resonance peak with highest intrinsic Q (narrower linewidth) for the small racetrack: (a) TM and (b) TE polarization.

V. Conclusion

We have experimentally demonstrated ultra-high-Q factors on racetrack resonators fabricated on a thick SOI platform by reducing the propagation losses of the waveguides through an MPW-compatible hydrogen annealing based sidewall roughness smoothing post-processing technique. For a racetrack with an area of $\sim$5.5 mm^2 we measured an intrinsic Q of 14.3×10^6, whereas for a smaller one with a $\sim$1.48 mm^2 area we measured 10.7×10^6. The estimated propagation losses extracted from the measured Q-factor was $\sim$2.7 dB/m. These ultra-low losses will potentially enable the development of emerging PIC applications, such as photonic quantum processors, and various photonic sensors.

References

[1] D. Melati, A. Melloni, and F. Morichetti, "Real photonic waveguides: Guiding light through imperfections," *Adv. Opt. Photon.*, vol. 6, no. 2, pp. 156–224, Jun. 2014, doi: 10.1364/AOP.6.000156.

[2] Y. A. Vlasov and S. J. McNab, "Losses in single-mode silicon-on-insulator strip waveguides and bends," *Opt. Exp.*, vol. 12, no. 8, pp. 1622–1631, Apr. 2004, doi: 10.1364/OPEX.12.001622.

[3] T. Aalto et al., "Open-access 3-μm SOI waveguide platform for dense photonic integrated circuits," *IEEE J. Sel. Topics Quantum Electron.*, vol. 25, no. 5, Sep./Oct. 2019, Art. no. 8201109, doi: 10.1109/JSTQE.2019.2908551.

[4] W. Jin et al., "Hertz-linewidth semiconductor lasers using CMOS-ready ultra-high-Q microresonators," *Nature Photon.*, vol. 15, no. 5, May 2021, Art. no. 5, doi: 10.1038/s41566-021-00761-7.

[5] T. J. Kippenberg, R. Holzwarth, and S. A. Diddams, "Microresonator-based optical frequency combs," *Science*, vol. 332, no. 6029, pp. 555–559, Apr. 2011, doi: 10.1126/science.1193968.

[6] N. T. Otterstrom, R. O. Behunin, E. A. Kittlaus, Z. Wang, and P. T. Rakich, "A silicon Brillouin laser," *Science*, vol. 360, no. 6393, pp. 1113–1116, Jun. 2018, doi: 10.1126/science.aar6113.

[7] D. Marpaung, J. Yao, and J. Capmany, "Integrated microwave photonics," *Nature Photon.*, vol. 13, no. 2, Feb. 2019, Art. no. 2, doi: 10.1038/s41566-018-0310-5.

[8] A. Orieux and E. Diamanti, "Recent advances on integrated quantum communications," *J. Opt.*, vol. 18, no. 8, Jul. 2016, Art. no. 083002, doi: 10.1088/2040-8978/18/8/083002.

[9] A. Belsley, E. J. Allen, A. Datta, and J. C. F. Matthews, "Advantage of coherent states in ring resonators over any quantum probe single-pass absorption estimation strategy," *Phys. Rev. Lett.*, vol. 128, no. 23, Jun. 2022, Art. no. 230501, doi: 10.1103/PhysRevLett.128.230501.

[10] T. Christopoulos, O. Tsilipakos, G. Sinatkas, and E. E. Kriezis, "On the calculation of the quality factor in contemporary photonic resonant structures," *Opt. Exp.*, vol. 27, no. 10, pp. 14505–14522, May 2019, doi: 10.1364/OE.27.014505.

[11] Y. Zhang et al., "Design and demonstration of ultra-high-Q silicon microring resonator based on a multi-mode ridge waveguide," *Opt. Lett.*, vol. 43, no. 7, pp. 1586–1589, Apr. 2018, doi: 10.1364/OL.43.001586.

[12] M. A. Guillén-Torres, M. Caverley, E. Cretu, N. A. F. Jaeger, and L. Chrostowski, "Large-area, high-Q SOI ring resonators," in *Proc. IEEE Photon. Conf.*, 2014, pp. 336–337. doi: 10.1109/IPCon.2014.6995381.

[13] S.-W. Huang, H. Liu, J. Yang, M. Yu, D.-L. Kwong, and C. W. Wong, "Smooth and flat phase-locked Kerr frequency comb generation by higher order mode suppression," *Sci. Rep.*, vol. 6, no. 1, May 2016, Art. no. 1, doi: 10.1038/srep26255.

[14] L. Zhang et al., "Ultrahigh-Q silicon racetrack resonators," *Photon. Res,* vol. 8, no. 5, pp. 684–689, May 2020, doi: 10.1364/PRJ.387816.

[15] L. Zhang et al., "Ultralow-loss silicon photonics beyond the Singlemode regime," *Laser Photon. Rev,* vol. 16, no. 4, 2022, Art. no. 2100292, doi: 10.1002/lpor.202100292.

[16] Y. Zhang, K. Zhong, X. Zhou, and H. K. Tsang, "Broadband high-Q multimode silicon concentric racetrack resonators for widely tunable Raman lasers," *Nature Commun.*, vol. 13, no. 1, Jun. 2022, Art. no. 1, doi: 10.1038/s41467-022-31244-0.

[17] A. Biberman, M. J. Shaw, E. Timurdogan, J. B. Wright, and M. R. Watts, "Ultralow-loss silicon ring resonators," *Opt. Lett.*, vol. 37, no. 20, pp. 4236–4238, Oct. 2012, doi: 10.1364/OL.37.004236.

[18] B. Zhang et al., "Compact multi-million Q resonators and 100 mhz passband filter bank in a thick-SOI photonics platform," *Opt. Lett.*, vol. 45, no. 11, pp. 3005–3008, Jun. 2020, doi: 10.1364/OL.395203.

[19] M.-C. M. Lee and M. C. Wu, "Thermal annealing in hydrogen for 3-D profile transformation on silicon-on-insulator and sidewall roughness reduction," *J. Microelectromech. Syst.*, vol. 15, no. 2, pp. 338–343, Apr. 2006, doi: 10.1109/JMEMS.2005.859092.

[20] S. Jeong and A. Oshiyama, "Complex diffusion mechanisms of a silicon adatom on hydrogenated Si(100) surfaces: On terraces and near steps," *Surf. Sci.*, vol. 433–435, pp. 481–485, Aug. 1999, doi: 10.1016/S0039-6028(99)00117-X.

[21] C. Bellegarde et al., "Improvement of sidewall roughness of submicron SOI waveguides by hydrogen plasma and annealing," *IEEE Photon. Technol. Lett.*, vol. 30, no. 7, pp. 591–594, Apr. 2018, doi: 10.1109/LPT.2018.2791631.

[22] Q. Wilmart et al., "A complete Si photonics platform embedding ultra-low loss waveguides for O- and C-band," *J. Light. Technol.*, vol. 39, no. 2, pp. 532–538, Jan. 2021, doi: 10.1109/JLT.2020.3030123.

[23] A. Bera, Y. Marin, M. Harjanne, M. Cherchi, and T. Aalto, "Ultra-low loss waveguide platform in silicon photonics," *Proc. SPIE*, vol. 12006, pp. 6–11, Mar. 2022. doi: 10.1117/12.2610022.

[24] Y. E. Marin, A. Bera, M. Cherchi, and T. Aalto, "Ultra-high-Q racetrack on thick SOI platform through hydrogen annealing," in *Proc. Eur. Conf. Opt. Commun.*, Basel, 2022, Art. no. We4E.3.

[25] R. A. Soref, J. Schmidtchen, and K. Petermann, "Large single-mode rib waveguides in GeSi-Si and Si-on-SiO_2," *IEEE J. Quantum Electron.*, vol. 27, no. 8, pp. 1971–1974, Aug. 1991, doi: 10.1109/3.83406.

[26] A. Melloni, P. Monguzzi, R. Costa, and M. Martinelli, "Design of curved waveguides: The matched bend," *J. Opt. Soc. Amer. A*, vol. 20, no. 1, pp. 130–137, Jan. 2003, doi: 10.1364/JOSAA.20.000130.

[27] M. Cherchi, S. Ylinen, M. Harjanne, M. Kapulainen, and T. Aalto, "Dramatic size reduction of waveguide bends on a micron-scale silicon photonic platform," *Opt. Exp.*, vol. 21, no. 15, pp. 17814–17823, Jul. 2013, doi: 10.1364/OE.21.017814.

[28] F. Gao, S. Ylinen, M. Kainlauri, and M. Kapulainen, "Smooth silicon sidewall etching for waveguide structures using a modified Bosch process," *J. MicroNanolithogr. MEMS MOEMS*, vol. 13, no. 1, Mar. 2014, Art. no. 013010, doi: 10.1117/1.JMM.13.1.013010.

[29] H. A. Haus, *Waves and Fields in Optoelectronics*. Hoboken, NJ, USA: Prentice Hall 1984.

Yisbel E. Marin received the M.Sc. degree in photonic networks engineering from Aston University, Birmingham, U.K., and Scuola Superiore Sant'Anna, Pisa, Italy, respectively, in 2015, and the Ph.D. degree in emerging digital technologies, photonics curriculum from Scuola Superiore Santa'Anna, Pisa, Italy, in 2019. She was a Postgraduate Research Fellow with the Optical Fiber Sensors- Integrated Photonics Subsystems Group, TeCIP Institute, Scuola Superiore Sant'Anna, working with optical fiber sensors and integrated photonics. She is currently a Research Scientist with the Silicon Photonics Group, VTT, working on PIC design and testing.

Arijit Bera received the M. Sc. in photonics, and the Ph.D. degree in silicon photonics from the Institute of Photonics, University of Eastern Finland, Joensuu, Finland, in 2013 and 2018, respectively. In 2018, he joined VTT, and has been with Silicon Photonics Team since 2020. During the Ph.D. degree and the years with VTT, he gained expertise in PIC design, and micro/nano fabrication of both active and passive photonic devices. He is currently with Quantum Photonics Team, VTT.

Matteo Cherchi received the M.Sc. degree in physics from the University of Pavia, Pavia, Italy, in 1997, and the M.Sc. degree in applied mathematics from the University of Cambridge, Cambridge, U.K, in 1998, and the Ph.D. degree in electronic engineering from the University of Palermo, Palermo, Italy. He was with Politecnico di Milano, Milan, Italy, and Pirelli focusing on basic research in photonics, and integrated photonic solutions, also in collaboration with the group of Prof. H. A. Haus from RLE (MIT). In 2011, he joined the Microphotonics Group with Prof. M. R. Watts, MIT, where he joined the Silicon Photonics Group, VTT, in 2011 .

Timo Aalto received the M.Sc. and D.Sc. degrees in optoelectronics technology from the Helsinki University of Technology, Espoo, Finland, in 1998 and 2004, respectively. Since 1997, he has been with VTT in the Micronova Clean Room Facility, in Espoo, Finland, with the primary research focus on silicon photonics. He has led VTT's Silicon Photonics R&D Team since 2006. He has authored approximately 100 refereed journal and conference papers, as well as one book chapter (three editions), and he is an in inventor for 11 granted patent families. He is the Member of SPIE, EOS and Photonics Finland. Relating to the successful business development in silicon photonics, he was the recipient of VTT Award 2014.